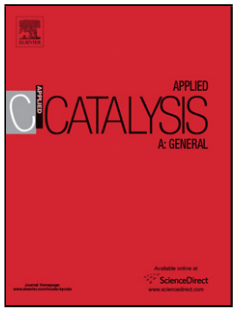

The consequences of support identity on the oxidative conversion of furfural to maleic anhydride on vanadia catalysts

Paola Santander (Conceptualization) (Methodology) (Software) (Formal analysis) (Investigation) (Data curation) (Writing - original draft) (Writing - review and editing) (Visualization), Luis Bravo (Software) (Investigation) (Data curation), Gina Pecchi (Resources) (Writing - review and editing), Alejandro Karelovic (Conceptualization) (Methodology) (Formal analysis) (Investigation) (Resources) (Writing - review and editing) (Supervision)

PII: S0926-860X(20)30106-X

DOI: https://doi.org/10.1016/j.apcata.2020.117513

Reference: APCATA 117513

To appear in: *Applied Catalysis A, General*

Received Date: 3 December 2019

Revised Date: 14 February 2020

Accepted Date: 5 March 2020

Please cite this article as: Santander P, Bravo L, Pecchi G, Karelovic A, The consequences of support identity on the oxidative conversion of furfural to maleic anhydride on vanadia catalysts, *Applied Catalysis A, General* (2020), doi: https://doi.org/10.1016/j.apcata.2020.117513

The consequences of support identity on the oxidative conversion of furfural to maleic anhydride on vanadia catalysts

Paola Santander[1,2*], Luis Bravo[1,2], Gina Pecchi[2,3], Alejandro Karelovic[1,2,4*]

[1]*Carbon and Catalysis Laboratory (CarboCat), Department of Chemical Engineering, University of Concepción, Concepción, Chile*

[2]*Millennium Nuclei on Catalytic Processes towards Sustainable Chemistry (CSC), Chile.*

[3]*Physical Chemistry Department, Faculty of Chemical Sciences, University of Concepción, Chile.*

[4]*Unidad de Desarrollo Tecnológico (UDT), Universidad de Concepción, Chile.*

[*] Corresponding authors: isantander@udec.cl, akarelov@udec.cl

Graphical Abstract

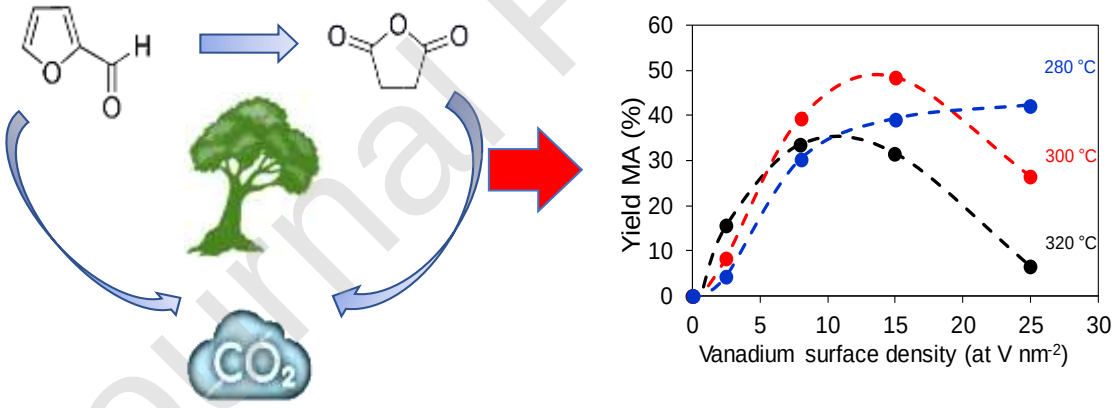

Highlights

- Vanadia supported on SiO_2, γ-Al_2O_3, ZrO_2 and TiO_2 with surface density from 0.5 to 25 at V nm^{-2}.
- Depending on reaction temperature and support nature, maleic anhydride yield is maximized for surface densities from 8 to 15 at V nm^{-2}.
- On the alumina and silica supported catalysts the activity mainly depends on the vanadia dispersion.
- Over partially reducible zirconia and titania supports, the yield toward maleic anhydride can be enhanced operating at oxygen lean conditions

Abstract

Maleic anhydride (MA) is a high value building block molecule whose synthesis from furfural (FUR) is proposed as a green and sustainable alternative. In this work, vanadia supported on SiO_2, γ-Al_2O_3, ZrO_2 and TiO_2 catalysts were synthetized, characterized and investigated for the selective gas phase oxidation of FUR to MA. The catalytic properties depend on both, the nature of the support and the vanadia surface dispersion. V_2O_5/SiO_2 and V_2O_5/γ-Al_2O_3 display ca. 50% MA yield. Conversely, for the V_2O_5/ZrO_2 and V_2O_5/TiO_2 catalysts, complete FUR oxidation to CO_2 and negligible MA production was obtained. By decreasing the oxidation potential of the reaction feed, V_2O_5/ZrO_2 and V_2O_5/TiO_2 catalysts achieve MA yields comparable to V_2O_5/SiO_2 and V_2O_5/γ-Al_2O_3 catalysts. This behavior is

attributed to the higher vanadia dispersion on ZrO_2 and TiO_2 and the reducible nature of these supports. The results obtained in this work offer new catalytic alternatives for the sustainable production of MA.

Key words: furfural, catalytic partial oxidation, maleic anhydride, selective oxidation, supported vanadia catalysts

1. Introduction

Depletion of fossil fuels and global warming has increased the importance of renewable resources and green technologies. In this context, biomass from lignocellulose, composed of 20% lignin, 30% hemicellulose and 45% of cellulose is a promissory sustainable alternative to produce fuels and chemicals. Although the most abundant material coming from biomass is cellulose, due to its complex nature and rigid structure its use is limited to the manufactory of paper and cardboard. Most of the used technologies for the conversion of lignocellulose into chemicals and fuels are dependent of the pretreatment to obtain cellulose from lignin destroying its rigid structure followed by an acid catalytic hydrolysis to transform cellulose into value-added products, the so-called platform molecules[1]. Within these products, we can find furfural (FUR), produced in large scale from agricultural residues of biomass, a valuable molecule because of the large variety of chemicals produced from it[2]. One of these value-added chemicals is maleic anhydride (MA), used in the manufacture of lubricant additives[3], unsaturated polyester resins[4], surface coatings[5], plasticizers[6], copolymers[7] and pharmaceuticals[8], among others. MA is commercially manufactured from the gas-phase oxidation of *n*-butane, a fossil fuel byproduct, using vanadyl pyrophosphate catalysts (VPO) [9].

Vanadium-based catalysts have attracted much attention because they have demonstrated to be one of the most efficient catalysts for partial selective oxidation of light alkanes, and also for its reasonable cost and environmental considerations. Among them, supported vanadia catalysts have been widely studied. Many efforts have been done in order to prepare efficient vanadium-based catalysts with high activity towards the selective oxidation of alkanes. Accordingly, it has been demonstrated that the vanadium in the 5+ oxidation state is necessary in the oxidation of alkanes. Likewise, the supports for vanadia and the preparation method also play an important role on the properties and catalytic performances for oxidation of light alkanes[10].

Benomar et al.[11] studied the catalytic performance of vanadium oxides supported on Al_2O_3 and/or ZrO_2 for the oxidative dehydrogenation of ethane and in the methanol aerobic transformation. They found that the catalytic performance depends on the nature of the metal oxide support. Accordingly, at high ethane conversion, the activity decreases in the order: VO_x/ZrO_2 > VO_x/(Al,Zr-oxides) > VO_x/Al_2O_3. However, at low and medium ethane conversions, the selectivity to ethylene presents an opposite trend: VO_x/Al_2O_3 > VO_x/(Al,Zr-oxides) > VO_x/ZrO_2. This behavior, at high ethane conversions, was attributed to a lower ethylene decomposition related to a better vanadium dispersion and a higher proportion of redox sites. Nevertheless, the inverse trend observed at low and medium conversion, is attributed to their low acid character, the formation of unselective V–O–Zr sites and the low vanadium dispersion capacity as a consequence of the low surface area of the supports.

On the other hand, Hu et al.[12] systematically studied the influence of different vanadium precursors on the structure−performance relationships of VO_X-SiO_2 catalysts. They used ammonium metavanadate (NH_4VO_3, V^{5+}), vanadium acetylacetonate [$V(acac)_3$, V^{3+}], and vanadyl sulfate ($VOSO_4$, VO^{2+}, V^{4+}) as vanadium precursors to prepare the catalysts. The

catalytic activity was tested in the propane dehydrogenation reaction. They found that the textural properties, dispersion of vanadium species and catalytic performance of the catalysts are influenced by the use of different vanadium precursors. They also found that when using NH_4VO_3 as the vanadium precursor, vanadium species, in the form of isolated species, are highly dispersed, presenting better catalytic performance. The catalysts derived from $V(acac)_3$, at low vanadium content present a more stable catalytic performance and lower deactivation rate, presumably due to the formation of low-polymerized vanadium species. However, with the increase of vanadium content, more polymeric vanadium species are formed on the catalysts in detrimental of their catalytic performance. In the case of $VOSO_4$ as the precursor, a low catalytic performance was found as a result of the formation of bulk crystalline V_2O_5 in the catalysts.

Love et al.[13] studied the anchoring and subsequent thermal reconstruction of vanadium oxide on amorphous silica by solvent-free vapor deposition of vanadium oxytriisopropoxide (VTI) on dehydrated silica. They found that when VTI is grafted to SiO_2, it reacts with both isolated silanols and strained siloxane bridges. Afterwards, calcination form transient V−OH species, which react with the silica surface to form isolated, tetrahedral VO_4 sites. They demonstrate that this anchoring procedure permits control the dispersion of two-dimensional metal oxide sites on a support material.

Even though several renewable routes to obtain MA from catalytic oxidation of FUR have been reported[2,14,15], most of them are performed in liquid phase involving the formation of several byproducts[16–18]. Lan et al.[16] reported that $H_5PV_2Mo_{10}O_{40}$ catalyst in combination with $Cu(CF_3SO_3)_2$ avoid the hydrolysis of maleic anhydride under P_{O2} of 20 atm at 110°C in an organic solvent (acetonitrile:acetic acid = 2:1.3 in volume) reaching 98% of FUR conversion after 14 h of reaction, 54% yield of MA and 7.5% for 5-acetoxyl-2(5H)-furanone production.

On the other hand, Li and co-workers carried out the catalytic conversion of FUR to MA using Mo_4VO_{14} during 16 h of reaction at 20 bar of O_2 and 120°C and acetic acid as solvent, reaching 100% FUR conversion with 62% yield of MA, and formic acid as major by-product with leaching of V and Mo[17]. Recently, Lv et al (2018) reported highly efficient vanadium oxide nanosheets on graphene oxide catalysts in the oxidation of hydroxy methyl furfural (HMF) with 99.8% of HMF conversion and 90.9% selectivity to MA at 4 h of reaction. The lower efficiency on FUR conversion, 90% of conversion and 60% of selectivity to MA at 12 h of reaction was attributed to the formation of a hydroxyfurfural intermediate in the reaction pathway[14]. In the case of HMF, the cleavage of C-C bond of the hydroxymethyl group and furan ring was favored due to the presence of the π-conjugated system making the C-C bond more easily to break, enhancing the reaction rate[18].

The good performance in the oxidation of HMF to MA of vanadium-based catalysts has been attributed to the strong Brønsted acid sites, allowing a fast desorption of the products, avoiding it's over oxidation to CO_2. Additionally, some catalysts with Keggin structure confer a high thermal stability demonstrating that the presence of V^{5+} is crucial because vanadium acts as coordinating site in selective oxidation processes[19].

Although, most of the studies have been performed in liquid phase, the continuous gas-phase oxidation process is foreseen as a better alternative because it offers several advantages such as use of low-cost air, less side products, versatility in operating temperatures and better catalyst recuperation[2].

There are only few works on the gas-phase oxidation of FUR to MA. Recently, Li et al. reported the catalytic gas phase oxidation of FUR to MA using vanadium phosphorous oxide obtaining 90% of FUR conversion at 360°C using 10 vol.% FUR in the feed with stable

activity during 25 h. The authors attributed the excellent performance to a high exposure of the (2 0 0) crystal plane of the VPO phase[20]. Ojeda et al. reported the effect of the vanadium structure (density in the range 0.5-25 V atoms nm^{-2}) for V_2O_5/γ-Al_2O_3 catalysts, being the well-dispersed vanadium oxide catalyst with density of 8 V atoms nm^{-2} the one with the best catalytic performance. They also report that if the catalyst is contacted with FUR at 240°C and then the temperature is increased stepwise, the initial conversion close to 50%, decreases to 20% due to resin deposition on the catalyst. Conversely, if the catalyst is initially contacted with FUR at 320°C, the temperature of full conversion, FUR conversion increases with a decrease in resin formation and hence lower deactivation rates. Nevertheless, at all reaction conditions, deactivation was evidenced on these V_2O_5/γ-Al_2O_3 catalysts[21,22].

According to the information presented above, supported vanadia catalysts has been shown to be active and selective for the partial oxidation of FUR to MA in gas phase. However, the influence of the support properties has not yet been studied. Herein we address the effect of the nature of support (SiO_2, γ-Al_2O_3, ZrO_2 and TiO_2) and the surface vanadium content (0.5, 2.5, 8, 15 and 25 V atoms nm^{-2}) on the partial catalytic oxidation in gas phase of FUR to MA. The results reported in this work demonstrate that the catalytic properties depend on nature of the support and the dispersion of the surface vanadium species. V_2O_5/SiO_2 and V_2O_5/γ-Al_2O_3 present better activity than V_2O_5/ZrO_2 and V_2O_5/TiO_2 catalysts under the studied conditions. However, V_2O_5/ZrO_2 and V_2O_5/TiO_2 increase their activity with the decrease in the oxidative conditions, promising to be a good alternative of heterogeneous catalysts for this reaction.

2. Experimental

2.1 Catalysts preparation

Supported vanadium oxide catalysts were prepared by wet impregnation at different surface concentration of vanadium (0.5, 2.5, 8, 15 and 25 atom V nm^{-2}) using ammonium metavanadate as precursor (NH_4VO_3, Sigma-Aldrich). The surface concentration is defined as the number of vanadium atoms per square nanometer of the catalyst and was calculated from the V_2O_5 content and the BET surface area. It is useful for comparing catalysts prepared on supports with different surface areas. At a given vanadium surface concentration, the resulting structure of vanadia species will depend on the ability the support to disperse the VOx species[23]. In order to achieve the atomic surface concentration as atom V nm^{-2}, prior to the synthesis the surface area of the supports was measured: i) SiO_2 (Saint-Gobain Norpro SS 61138, 231 $m^2\,g^{-1}$), ii) γ-Al_2O_3 (Saint-Gobain Norpro SA 6173, 212 $m^2\,g^{-1}$), iii) ZrO_2 (56 $m^2\,g^{-1}$. Saint-Gobain Norpro SZ 31163) and iv) TiO_2 (50 $m^2\,g^{-1}$. Evonik P-25). Table 1 shows V surface density and the corresponding V_2O_5 loading (wt.%) of the synthesized catalysts. Oxalic acid (Merck-Millipore) was used for NH_4VO_3 dissolution by forming a vanadium-oxalate complex with an oxalic acid/ NH_4VO_3 molar ratio of 2[24]. For the synthesis of this complex, an adequate amount of oxalic acid was dissolved in hot distilled water and maintained in a water bath at 80°C under a continuous stirring of 700 rpm. The metavanadate was gradually added until a dark blue dissolution was obtained. Once the oxalate-vanadium complex was formed, the dissolution was cooled down to room temperature, maintaining the agitation to avoid precipitation. Finally, the dissolution was mixed with the support and dried under vacuum in a rotary evaporator at 58°C during 2 h. The impregnated solids were dried overnight at 105°C and calcined in static air at 500°C for 3 h at a heating rate 10°C min^{-1}.

Additionally, bulk V_2O_5 was prepared by calcination of NH_4VO_3 at 500°C (10°C min^{-1}) in static air during 1 h.

Table 1. Nominal V_2O_5 content (wt. %) in the V_2O_5 supported catalysts as a function of vanadium atom density.

at V nm^{-2}	wt % V_2O_5			
	SiO_2	γ-Al_2O_3	ZrO_2	TiO_2
0.5	1.7	1.7	0.5	0.6
2.5	8.0	8.0	2.0	3.0
8	22	21	6.7	8.6
15	34	34	12	15
25	46	46	18	23

2.2 Catalytic activity

FUR oxidation was performed in a tubular fixed-bed stainless-steel reactor (length 60 cm, internal diameter 0.78 cm) placed inside of an electric oven. The catalytic bed was prepared mixing quartz sand (0.4 g, 150-380 μm particle size) with the catalyst (40 mg, 150-380 μm particle size) which resulted in a catalytic bed of ca. 5 mm in length, well inside the isothermal section of the electric oven. The catalyst was placed in the center of the reactor and was held by quartz wool.

Before the reaction, the catalyst was *in situ* pre-treated in air flow (21% vol O_2/N_2, 20 mL min^{-1}) at 350°C for 1 h at a heating rate of 10°C min^{-1}. Then, the temperature was adjusted to the desired value, the O_2/FUR molar ratio was set to 20 (P_{FUR}= 0.084 kPa, P_{O2}= 1.68 kPa), a flow of argon (2 mL min^{-1}) was used as internal standard and the mixture of gases, total flow of 22 mL min^{-1} was conducted through the catalytic bed. The concentration of FUR (Merck-Millipore) in the gas phase was controlled using a stainless-steel saturator submerged in a thermostated bath at 30 °C and N_2 (5 mL min^{-1}) was used as carrier gas by bubbling into the saturator. We checked that the saturator worked at thermodynamic equilibrium conditions by varying the carrier gas flow rate, which did not produced a variation in the concentration of FUR. The N_2, Ar and air flows were controlled by mass flow controllers (Kofloc 8500).

The concentrations of reagents and products were measured online using a quadrupole mass spectrometer (Omnistar GSD 320) which was connected with a tee at the exit of the reactor. For each compound, the main ions according with most abundant m/z (mass-to-charge ratio) fragment were identified. The fragments m/z= 95 for FUR, m/z= 26 for MA and m/z= 40 for Ar were chosen in order to avoid the overlapping of signals. All transfer lines were held at 100°C to prevent condensation of reactants and products. For instance, the MA vapor pressure at 100°C is 3.43 kPa, which is well above the inlet FUR pressure (0.084 kPa) and hence the maximum attainable MA concentration. The raw MS intensities of reagents and products were normalized by that of the internal standard (Ar). FUR conversion and MA yield were calculated according to equations 1 and 2, respectively.

$$X_{FUR} = \frac{FUR_{in} - FUR_{out}}{FUR_{in}} \times 100 \qquad \text{Eq. 1}$$

$$Y_{MA} = \frac{MA_{out}}{FUR_{in}} \times 100 \qquad \text{Eq. 2}$$

were FUR_{in} and FUR_{out} are the inlet and outlet furfural molar flow rate, respectively, and MA_{out} is the outlet molar flow rate of MA.

The evolution of the reaction temperature during a catalytic run start at 320°C, then decreased to 300°C, followed to 280°C and finally increased again to 320°C to study possible catalyst deactivation. Each temperature was maintained for at least 4 h.

2.3 Characterization

X-Ray diffraction (XRD) analyses were performed in an X-ray diffractometer Bruker D4 Endeavor (Billerica, USA) with a solid-state detector (LynxEye) in the range of 2θ = 5-90°.

UV-vis diffuse reflectance spectroscopy (DRS) was performed in a Thermo Scientific Evolution 260 Bio spectrometer equipped with a Spectralon-coated integrating sphere ISA 220. The spectra were recorded in the range of 190 and 1100 nm using a Spectralon discs as a standard.

Thermogravimetric analyses (TGA) under controlled atmosphere were performed in a Cahn-Versatherm thermogravimetric analyzer with a sensitivity of 0.1 μg in the range of 25-800°C at a heating rate of 5 °C min^{-1} under air flow of 100 mL min^{-1}.

Textural properties were determined prior degassing at 200°C during 4 h by adsorption-desorption isotherms at 77 K in a Gemini VII Surface Area Analyzer Micromeritics (Georgia, USA). Surface area was calculated from BET equation and the pore size distributions obtained from the desorption branch of the nitrogen isotherms using Barrett-Joyner-Halenda (BJH) method.

The acid properties were characterized by means of NH_3 temperature programmed desorption (TPD). Samples (ca. 0.05 g) were pretreated under He flow at 110°C with a heating rate of 10°C min^{-1}. The pretreatment was performed during 30 min using a He flow of 50 mL min^{-1}. The surface was saturated with ammonia at 110°C by injecting 0.5 mL pulses of pure NH_3 gas. The area of the NH_3 effluent was followed by a TCD. The saturation was thus ensured by performing at least 10 pulse injections and verifying that the peak area reached a constant value. After saturation, weakly adsorbed NH_3 was removed under He flow (50 mL min^{-1}) at 110°C during 30 min and afterward, the system was cooled to room temperature and the desorption process was carried out at a heating rate of 10°C min^{-1} from 110°C to 900°C. TPD curves were recorded by a TCD.

3. Results and discussion

3.1 Catalytic activity

Fig. S1 shows the mass spectrometry data corresponding to the MA signal corrected by Ar (m/z= 26/40) of each family of catalysts. The spectrograms present the evolution of the MA signal as a function of reaction temperature, which decreases from 320°C to 280°C and finally increases again to 320°C. When the temperature is restored to 320°C, it reaches similar MA yields compared to that at the beginning of the reaction. This means that deactivation of the catalysts is minimal.

Moreover, additional m/z fragments characteristic of other possible reaction products, such as furan (m/z = 68 and 39) were followed. No significant concentrations of furan were detected. In the case of CO_2 (m/z = 44), it was detected but not quantifiable within an acceptable precision due to the contributions of FUR and MA.

Fig. 1 shows the MA yield as a function of V surface density for the synthesized catalysts at the reaction temperatures of 280°C, 300°C and 320°C. It can be seen that V_2O_5/SiO_2 and $V_2O_5/\gamma\text{-}Al_2O_3$ (Fig. 1a and 1b) are significantly more active in terms of MA yield with regard to V_2O_5/ZrO_2 and V_2O_5/TiO_2 (Fig. 1c and 1d) catalysts.

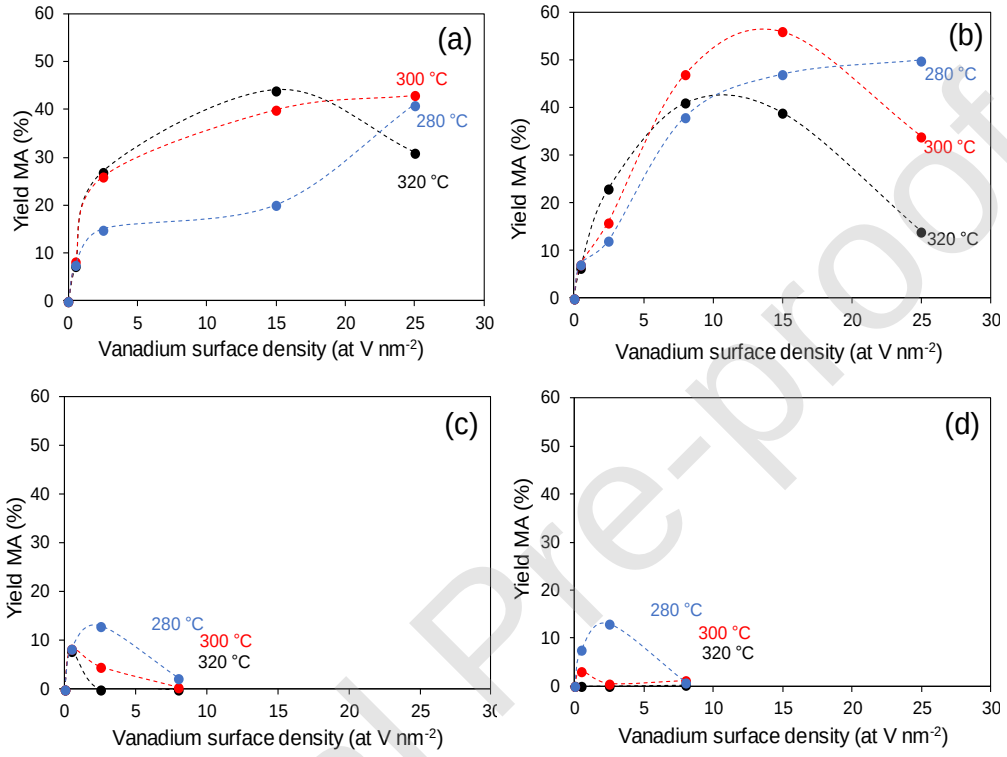

Figure 1. Yield of MA as a function the vanadium density of: (a) SiO_2, (b) Al_2O_3, (c) ZrO_2 and (d) TiO_2 vanadia-supported catalysts at different reaction temperature. (P_{FUR}= 0.084 kPa, P_{O2}= 1.68 kPa, O_2/FUR=20, GHSV= 550 mL min^{-1} g^{-1}).

At 280°C both V_2O_5/SiO_2 and $V_2O_5/\gamma\text{-}Al_2O_3$ show a continuous increase in MA yield as a function of V surface density, and when the reaction temperature is augmented to 300°C, a maximum MA yield is observed for the 15 at. V nm^{-2} $V_2O_5/\gamma\text{-}Al_2O_3$ catalyst. Further increase in surface V species is detrimental for MA production and at 320°C the behavior is qualitatively similar with the maximum MA yield lowered to 8 at. V nm^{-2}. Interestingly, the behavior for V_2O_5/SiO_2 is quite similar to $V_2O_5/\gamma\text{-}Al_2O_3$, namely a maximum starts to

develop when the temperature is increased and shifted towards higher V concentrations compared to $V_2O_5/\gamma\text{-}Al_2O_3$. Thus, at 320°C for V_2O_5/SiO_2 the maximum is located at 15 at. V nm^{-2} whereas for $V_2O_5/\gamma\text{-}Al_2O_3$ at 8 at. V nm^{-2}, in line with previous reported by Ojeda et al. for $V_2O_5/\gamma\text{-}Al_2O_3$[22]. With regard to MA formation, similar values were obtained for $V_2O_5/\gamma\text{-}Al_2O_3$ and V_2O_5/SiO_2 with 49% and 36% respectively. This result shows that, in spite of the differences in the acid-base properties of silica and alumina, $V_2O_5/\gamma\text{-}Al_2O_3$ and V_2O_5/SiO_2 catalysts present a similar catalytic behavior in the partial FUR oxidation in gas phase. The maximum MA productivity was attained for $15V\gamma\text{-}Al_2O_3$ catalysts that presents 55% MA yield which is equivalent to a space time yield of 60 $g_{AM}\ g_{cat}^{-1}\ h^{-1}$.

Interestingly, very low yields of MA were obtained when vanadia is supported on TiO_2 and ZrO_2, compared to SiO_2 and $\gamma\text{-}Al_2O_3$. At high reaction temperature (300°C and 320°C) MA yield was negligible for V_2O_5/TiO_2 and V_2O_5/ZrO_2 catalysts, and only at 280°C a maximum of 13% MA yield was evidenced for the catalyst with 2.5 at. V nm^{-2}. The lower MA yield for these catalysts is attributed to the complete oxidation of the organic compounds into CO_2 and H_2O (Fig. S2). This behavior can be attributed to the higher reaction rate that enables the further oxidation of MA towards consecutive products. In fact, it has been recognized the ability of ZrO_2 and TiO_2 to exchange surface O atoms, allowing the effectively participation of these supports in the oxidation reactions and consequently lead to the complete oxidation of the reactant[25,26]. Fig. S2 shows the experimental m/z 44/40 data. It can be seen an increase of the CO_2 production with the reaction temperature and non-deactivation of the catalysts.

The decrease in the MA yield for the catalysts with higher V density (>8 at V nm^{-2}) indicates that the presence of larger amount of VOx favor the MA oxidation to other products

such as CO and CO_2. This result is also supported in Fig. 2 that shows that CO_2 production increases with vanadium surface density. Even though, in Fig. 2 is also seen that for 100% FUR conversion at higher vanadium loading, MA yield decreases with no changes in the CO_2 formation maintained in a high level. This result is a clear indication that consecutive formation of CO_2 occurs via oxidation of MA. A simplified reaction scheme is proposed:

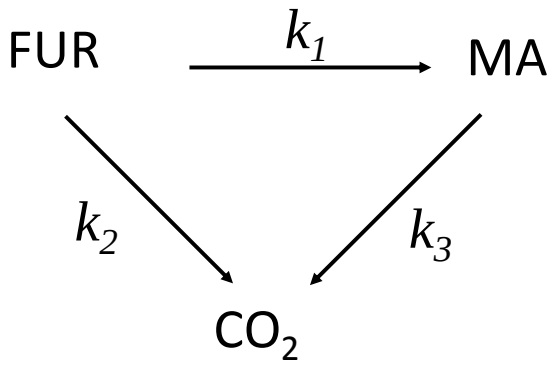

Scheme 1. Proposed reaction pathway for FUR oxidation on supported vanadia catalysts

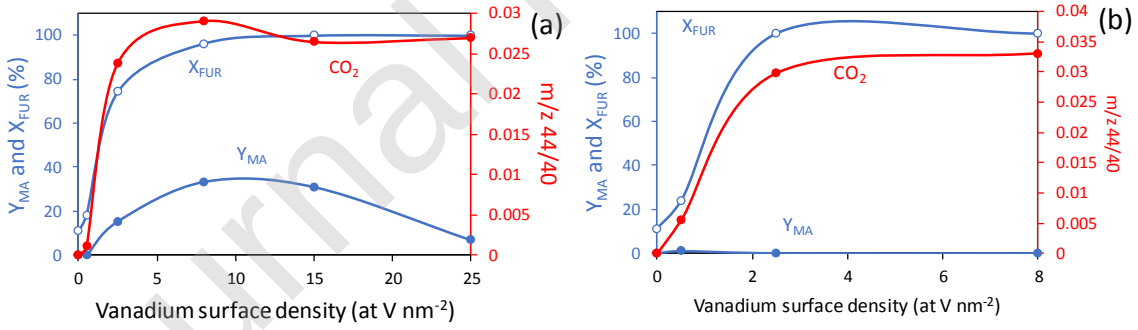

Figure 2: Evolution of MA yield (Y_{MA}), FUR conversion (X_{FUR}) and CO_2 production (expressed as m/z = 44/40) as a function of vanadium surface density for: (a) V_2O_5/γ-Al_2O_3 and (b) V_2O_5/ZrO_2 catalysts at 320°C. (P_{FUR}= 0.084 kPa, P_{O2}= 1.68 kPa, O_2/FUR=20, GHSV= 550 mL min^{-1} g^{-1})

As observed in Fig. 2b, at the same reaction conditions, the catalytic performance of V_2O_5/ZrO_2 is much more favourable towards total oxidation of the organic compounds than $V_2O_5/\gamma\text{-}Al_2O_3$ catalyst. This trend certainly indicate that the tuning of the rate constants or reactant concentration is necessary for attaining high MA selectivity.

Therefore, one strategy to increase the MA yield is to decrease the oxygen concentration in order to favor the partial oxidation reactions. Consequently, For V_2O_5/TiO_2 and V_2O_5/ZrO_2 catalysts, the O_2/FUR molar ratio in the feed was decreased from 20 to 10 and 2.5, and the experimental results are shown in Fig. 3.

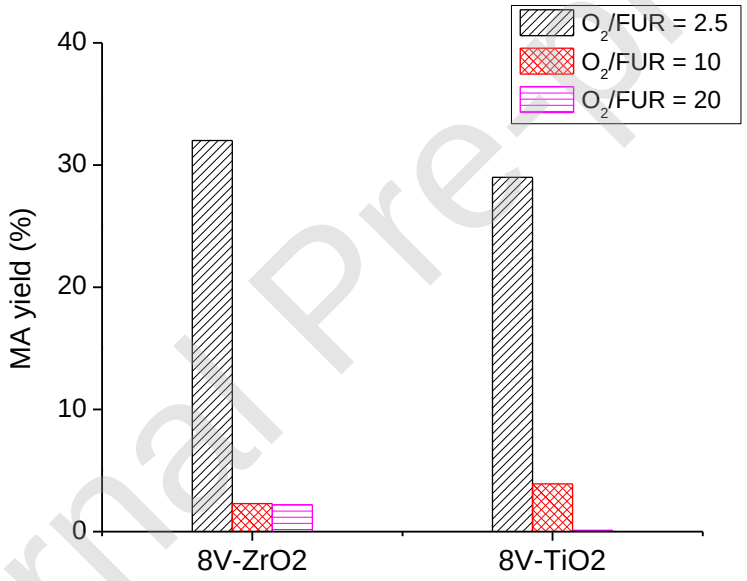

Figure 3. Effect of the O_2/FUR ratio on the MA yield for 8V-ZrO_2 and 8V-TiO_2 catalysts. (P_{FUR}= 0.084 kPa, GHSV= 550 mL min^{-1} g^{-1}, 280°C)

Fig. 3 shows that for 8V-ZrO_2 and 8V-TiO_2 catalysts, MA yield increases markedly when O_2/FUR ratio decreases from 20 to 2.5, reaching MA yields closer to those obtained for V_2O_5/SiO_2 and $V_2O_5/\gamma\text{-}Al_2O_3$ catalysts at O_2/FUR ratio of 20. This result confirms the hypothesis that the vanadium ZrO_2 and TiO_2 supported catalysts are highly active in the gas

phase oxidation of FUR and to increase the selectivity towards MA is necessary to decrease the oxidation potential of the gas phase.

The previous discussion underlines the important effect of the nature of the support on the catalytic properties of the vanadium supported catalysts. In the following sections, we present the characterization of the materials in order to understand the kinetic results in light of their physicochemical properties.

3.2 XRD

Fig. 4 shows the XRD patterns of the vanadium-supported catalysts. As expected, the absence of well-defined diffraction peaks is observed in the case of catalysts with low vanadia content for SiO_2 support (ICSD 98-016-2617) which is in line with the well know amorphous structure of SiO_2. For the other supports, crystalline structures were observed, namely, γ-Al_2O_3 (ICSD 98-006-6559), monoclinic ZrO_2 (ICSD 98-008-0047) and for TiO_2 a mixture of anatase (ICSD 98-020-2243) and rutile (ICSD 98-016-5920) is observed. The absence of diffraction peaks attributed to vanadium phases at low densities, indicate nanostructured phases with too small crystal size, amorphous or either. This behavior is further analyzed by UV-vis analyses in the next section.

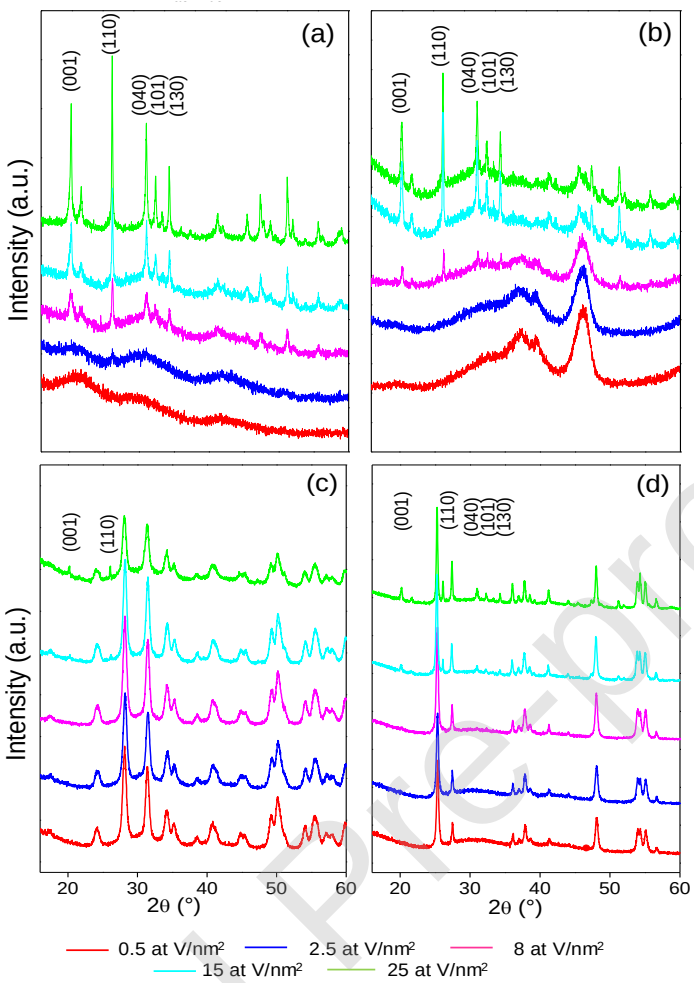

Figure 4. XRD patterns of V_2O_5 supported catalysts on (a) SiO_2, (b) γ-Al_2O_3, (c) ZrO_2, (d) TiO_2.

Significant differences can be seen in Fig. 4 regarding the vanadium loading at which the V_2O_5 crystallites start to appear in the XRD patterns. In the case of SiO_2 and Al_2O_3, orthorhombic V_2O_5 crystallites, (ICSD 98-009-9808) are observed at contents ≥ 8 at V nm^{-2} and for ZrO_2 and TiO_2, V_2O_5 crystals are detected only for densities ≥ 15 at. V nm^{-2}. This result underlines the easier agglomeration of vanadia on Al_2O_3 and SiO_2 compared to ZrO_2 and TiO_2. This is evident since at the same theoretical vanadium density (8 at. V nm^{-2})

orthorhombic V_2O_5 crystallites are detected by XRD on the former supports but cannot be detected on ZrO_2 and TiO_2. They cannot be detected by XRD because of their low concentration, poor crystallinity or small numbers of unit cells[23]. These results agree with similar catalysts prepared by Iglesia et al. [23] who showed that V_2O_5 crystallites appeared at the lower concentrations in the case of SiO_2. Our results are similar to those presented earlier by Ojeda et al. [21]. They showed that V_2O_5/γ-Al_2O_3 catalysts with loadings higher than 8 at. V nm^{-2} presented noticeable diffraction peaks attributable to bulk V_2O_5 crystals. However, Raman analyses showed that these crystals are also present on samples with lower V densities.

Table 2 summarizes the mean crystallite sizes for the detected orthorhombic V_2O_5 calculated from Scherrer equation[27]. It can be seen similar crystal sizes with not a clear dependence with the support nature and vanadium loading. Therefore, considering that slight differences can be attributed to the error of the calculation method, the similar values indicate almost no dependence with the nature of the support and vanadium content. These findings are in line with Kaichev and co-workers[28] based on Raman spectra, that report surface crystalline V_2O_5 with an orthorhombic structure for 15 and 20 at. V nm^{-2} on SiO_2 and γ-Al_2O_3 respectively, and a monolayer of isolated monomeric vanadium oxide species (VO_x) with vanadium in a tetrahedral oxygen environment for TiO_2 and ZrO_2. It is likely that with the increase of vanadium content, dimers and polymeric forms of $(VO_x)_n$ in an octahedral oxygen environment are formed being detected only after the filling of the monolayer coverage[28].

Therefore, in the synthesized catalysts, it can be assumed a monolayer formation of monomeric and polymeric vanadium oxides for ZrO_2 and TiO_2 catalysts whereas crystalline

V_2O_5 formation are present for the Al_2O_3 and SiO_2 catalysts at vanadium densities up to 8 at V nm^{-2}.

Table 2. Crystallite sizes determined by Scherrer equation of the detected orthorhombic V_2O_5 in the V_2O_5 supported catalysts.

at V nm^{-2}	d_{110} (nm)			
	SiO_2	Al_2O_3	ZrO_2	TiO_2
0.5	-	-	-	-
2.5	-	-	-	-
8	40	56	-	-
15	52	52	42	70
25	55	50	40	65

3.3 UV-Vis DRS

DR UV-Vis spectra were obtained for all of the studied catalysts and the absorbance spectra are summarized in Fig. S3. The Kubelka-Munk spectra for catalysts with vanadium density of 2.5 at V nm^{-2} are shown in Fig. 5a. The results are in line with previously results reported for these materials[23,29,30]. Within these works, Iglesia et al. studied the effect of the support nature (Al_2O_3, SiO_2, HfO_2, TiO_2, and ZrO_2) on the catalytic performance of supported vanadia in the oxidative dehydrogenation of propane. In the UV-visible diffuse reflectance spectra appear the expected bands in the 2–4 eV energy range attributed to O^{2-} to V^{5+} ligand to-metal charge transfer transitions. Additionally, due to an increase in the size and dimensionality of VOx domains, a decrease in the edge energy with increasing VOx surface density was detected for the studied supports[23]. On the other hand, Bulánek and co-workers

studied V-containing high-surface mesoporous siliceous materials and report bands in the region of 1.46–6.5 eV, attributed to charge transfer transitions of the $O \rightarrow V^{+5}$ type or to the d-d transitions of V^{+4} [29]. In the same way, Hidalgo et al. for vanadium supported on hydrotalcite, Al_2O_3, TiO_2 and SBA-15 catalysts report several bands in the range of 2-6 eV, attributed to ligand to metal charge-transfer transition of the $O \rightarrow V^{+5}$ type[30].

Therefore, considering the previous discussion, the several absorption bands in the region of 2–6 eV obtained in the UV-vis spectra in Fig. 5a can be attributed to the ligand to metal charge-transfer transition of the O^{-2} to V^{+5}. Since these charge transfer bands are broad, from the maximum absorption energy is difficult to define the exact position of the band. Consequently, the absorption edge calculated using the Tauc law, can be used to describe the near-edge region in amorphous semiconductors and the band gap transitions in crystalline semiconductors[31]. The edge energy (ε_o) is obtained from the intercept of a straight line of the first inflection of the function $[F(R_\infty)h\nu]^2$ plotted versus $h\nu$, where $F(R_\infty)$ is a Kubelka–Munk function and $h\nu$ is the energy of the incident photon (Fig. 5b)[29]. It can be seen that for the 2.5 at V nm^{-2} catalysts, the charge transfer band for SiO_2, Al_2O_3 and ZrO_2 appears at higher energies and do not interfere with the analysis of absorption edge regions corresponding to vanadium centers. Conversely, for the TiO_2 catalyst this band appears at 3.2 eV and overlaps with the corresponding vanadium bands, therefore it was necessary to subtract the TiO_2 bands for the 2.5 at V-TiO_2 catalyst (Fig. 5b).

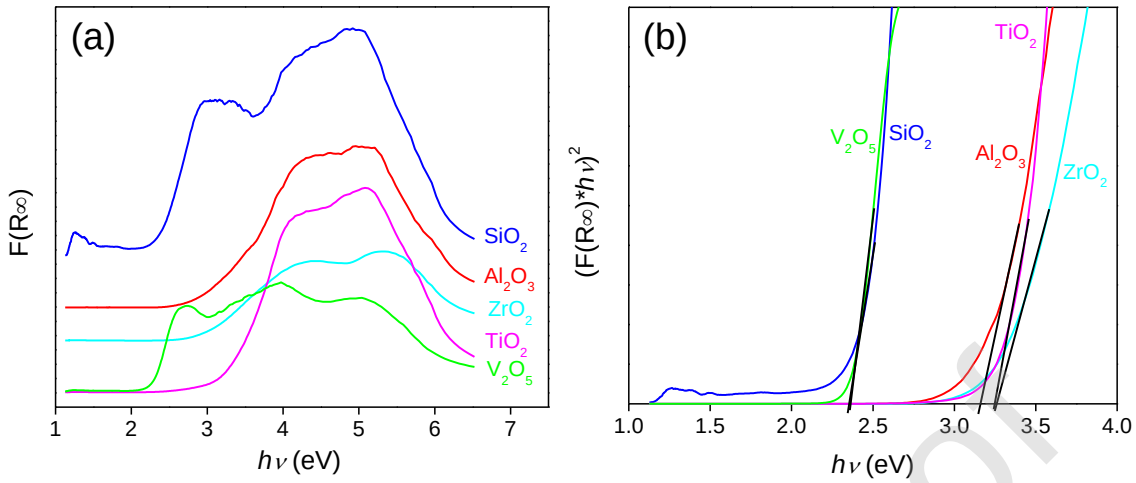

Figure 5. (a) DR UV-Vis spectra of 2.5 at V nm^{-2} catalysts and pure V_2O_5; (b) absorption edge energy calculated using the Tauc law.

In Fig. 6 is shown the effect of the vanadium surface density on the absorption edge energy for the V_2O_5 supported catalysts. For a better comparison, it is also shown as a horizontal black line the absorption energy of the bulk V_2O_5 (2.4 eV) calculated using Tauc law. It can be seen larger values of ε_o for the lowest vanadium content and a continuous decrease with the vanadium content. This behavior is in line with previous reports attributing this decrease to an increase in the size of the vanadium domains, getting close to the bulk value[23,29,30]. Additionally, the calculated ε_o values shown in Fig. 6 can be used as an indirect measurement of the vanadium dispersion. Therefore, the larger values of ε_o for the lower surface density (< 8 at V nm^{-2}) for Al_2O_3, ZrO_2 and TiO_2 indicate a high vanadia dispersion, whereas SiO_2 displays an ε_o value closer to the bulk V_2O_5 in all the range of vanadium concentrations, indicative of a lower vanadia dispersion. This finding, supported by XRD, indicates that SiO_2 presents lower effective vanadium dispersion, forming V_2O_5 crystals detected by XRD for V concentrations higher than 8 atV nm^{-2}. Therefore, the higher catalytic activity of V_2O_5/γ-Al_2O_3 catalysts compared to V_2O_5/SiO_2 catalysts is likely due to a higher vanadium

dispersion on γ-Al_2O_3. Additionally, the larger vanadia dispersion on V_2O_5/TiO_2 catalysts, is evidenced in the whole range of vanadium concentration since the bulk value is reached only at 25 at V nm^{-2}.

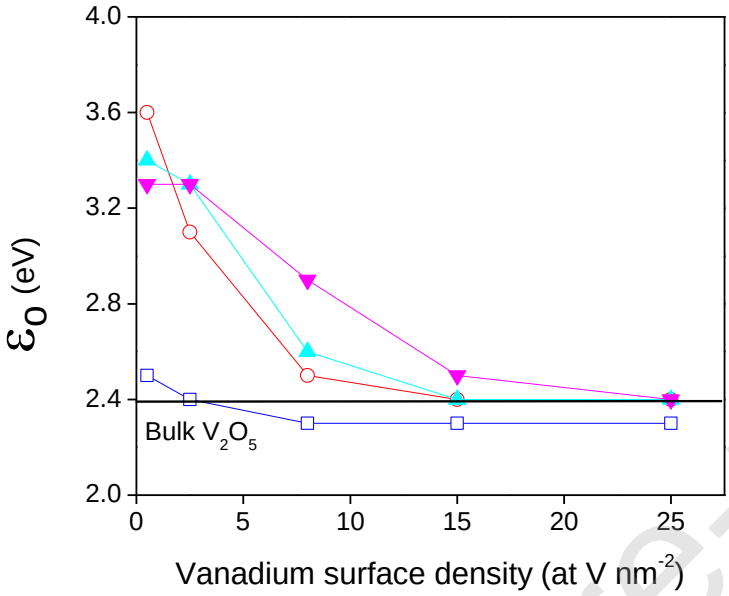

Figure 6. Absorption edge energy (ε_0) as a function of vanadium surface density for (□) SiO_2, (○) γ-Al_2O_3, (▲) ZrO_2 and (▼) TiO_2 catalysts. For a better comparison, the edge energy of the bulk V_2O_5 is shown as a horizontal line.

3.4 Thermogravimetric analysis (TGA).

The TGA profiles of the 25 atV nm^{-2} catalysts indicate two zones of weight loss up to 800°C (Fig S4). The first one between 90°C and 150°C corresponds to desorption of physisorbed species attributed to the evaporation of the solvent with a weight loss of approximately 10%. The second one corresponds to an important weight loss between 150°C and 250°C, which is attributed to the decomposition in one step of the organic matter[21]. The nominal weight reduction of the oxalate-vanadium precursors for the 25 atV nm^{-2}, assuming formation of V_2O_5/supported catalysts are shown in Table S1. The experimental values fit quite well with

the nominal values within 7% of uncertainty. Therefore, at calcination temperatures higher than 300°C the formation of V_2O_5 can be assumed for all the synthesized catalysts.

3.5 Textural properties

Fig. S5a shows that the N_2 adsorption isotherms for all the samples are type IV according to the IUPAC classification, with hysteresis loops characteristic of mesoporous materials[32]. The pore size distribution was estimated with the BJH method[33] that is suitable to calculate pore volume of a number of mesopores materials with a wide range of pore size[34,35] assuming cylindrical and open-ended pores. The pore size distribution indicates for silica, alumina and zirconia a narrow distribution centered at ca. 10 nm and broader for titania (Fig S5b).

Comparing the pristine and thermally treated support (500°C for 3 h) it was possible to observe that the surface area did not change significantly after calcination for Al_2O_3 (228 m^2 g^{-1} before calcination and 212 m^2 g^{-1} after calcination) and SiO_2 (before: 229 m^2 g^{-1}, after: 231 m^2 g^{-1}). However, ZrO_2 (before: 61 m^2 g^{-1}, after: 56 m^2 g^{-1}) and TiO_2 (before: 80 m^2 g^{-1}, after: 50 m^2 g^{-1}) did show a more significant reduction of the surface area after thermal treatment.

Fig. 7 shows the surface area (Fig. 7a) and pore diameter (Fig. 7b) as a function of vanadium surface density. The specific BET areas show a decrease with V_2O_5 content depending the nature of the support. For SiO_2 and γ-Al_2O_3 the large decrease in the surface area with the vanadium content can be attributed to partially blocking of the pores[21] or sintering of the support after the calcination[36]. These results are in line with Danilevich et al[37] that report that the decrease in the surface area with the vanadium content is larger in amorphous supports

such as SiO_2 and Al_2O_3[37]. In the case of ZrO_2 and TiO_2 catalysts, the surface areas do not vary significantly with vanadium loading compared to SiO_2 and Al_2O_3. Iglesia et al. [23] also observed that the increase in vanadium loading does not lead to a decrease in surface area for certain supports, and even reported an increase in surface area with vanadium loading in the case of ZrO_2.

With regard to the mean pore diameter, the low variation as a function of vanadium density, indicates that the decrease in the surface area is a consequence of vanadium layer that block some pores and keep the rest completely unblocked. Therefore, the previous discussion regarding to slight changes in the N_2 adsorption isotherms and pores size distribution after the incorporation of vanadium is indicative that the supports are mainly formed by a mesoporous structure.

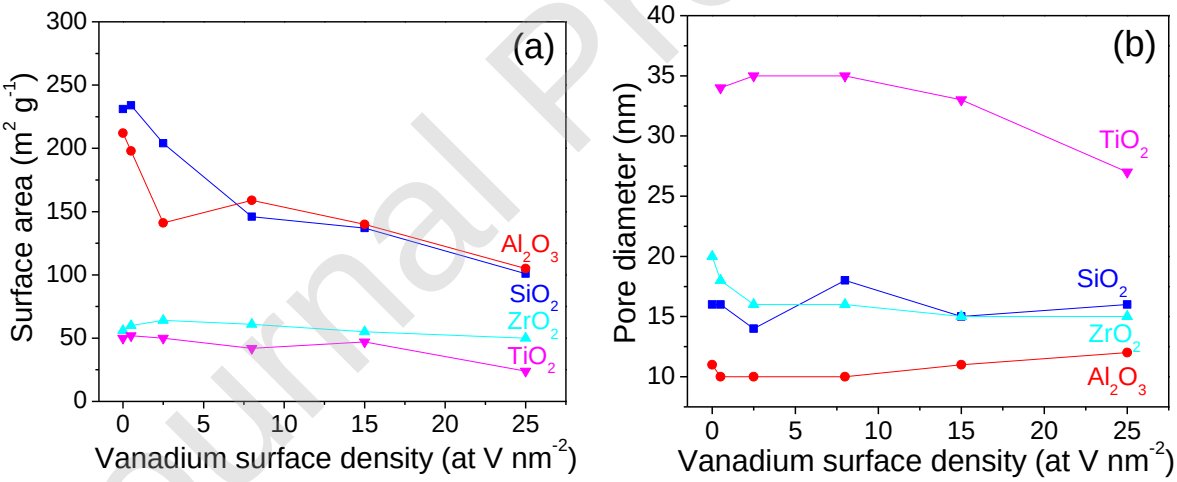

Figure 7. (a) Surface area; (b) mean pore diameter as a function of vanadium surface density.

3.6 Temperature programmed desorption (TPD) of NH_3

NH_3-TPD analyses were performed to study the acid properties of the 8 atV nm^{-2} catalysts. In Fig S6 it is possible to observe that the V_2O_5/γ-Al_2O_3 catalyst presents a broad NH_3

desorption peak in the range of 100°C to 400°C corresponding to the intermediate and stronger acid sites with a maximum of desorption at 200°C. The V_2O_5/ZrO_2, V_2O_5/SiO_2 and V_2O_5/TiO_2 catalysts do not show significant NH_3 desorption bands in the studied desorption temperature. Regarding the previous discussion of the catalytic results, this result show that acidity is not a key factor governing the activity of the studied catalysts for gas phase FUR oxidation to MA.

Conclusions

The nature of the support and the vanadium loading play an important role in the catalytic activity of the vanadia based catalysts for FUR oxidation to MA. Large differences in the performance of V_2O_5/SiO_2 and $V_2O_5/\gamma\text{-}Al_2O_3$ with regard to V_2O_5/ZrO_2 and V_2O_5/TiO_2 catalysts were detected. The catalysts supported on ZrO_2 and TiO_2, which are known to have the ability of exchange oxygen atoms, confer high reactivity, conducting to a complete oxidation of organic compounds into CO_2 and H_2O. We demonstrate that by decreasing the oxidation potential of the gas phase, the MA yield increased from near zero at O_2/FUR = 20 and 320°C, to ca. 30% at O_2/FUR = 2.5 and 280°C for ZrO_2 and TiO_2 catalysts, making them a good alternative to perform more ecofriendly processes.

Regarding V_2O_5/SiO_2 and $V_2O_5/\gamma\text{-}Al_2O_3$ catalysts, MA yield increases steadily with V surface density up to 8 and 15 at V nm^{-2}. At higher V loadings, MA yields decrease due to consecutive reactions that decompose MA. This maximum in activity depends on the temperature and vanadium dispersion. The larger activity in terms of MA yields at lower

temperature for $V_2O_5/\gamma\text{-}Al_2O_3$ compared to V_2O_5/SiO_2 is attributed to the higher vanadium dispersion on γ-alumina. Due to the fact that differences in the acidic properties measured by TPD-NH_3 do not correlate with catalytic activity, it can be concluded that for oxidation-inert supports such as Al_2O_3 and SiO_2, the activity is governed by the dispersion of vanadium species whereas for ZrO_2 and TiO_2, the much higher reactivity observed suggest that these supports are participating in the catalytic cycle. Further studies are needed to find the exact nature of the active sites and thus the nature of the oxygen species participating in the reaction.

CRediT author statement

Paola Santander: Conceptualization, methodology, software, formal analysis, investigation, data curation, writing – original draft preparation, writing – review & editing, visualization. **Luis Bravo:** Software, investigation, data curation. **Gina Pecchi:** Resources, writing – review & editing. **Alejandro Karelovic:** Conceptualization, methodology, formal analysis, investigation, resources, writing – review & editing, supervision.

Acknowledgements

Funding from Millennium Science Initiative of the Ministry of Economy, Development and Tourism, Chile grant Nuclei on Catalytic Processes towards Sustainable Chemistry (CSC) and CONICYT PIA/APOYO CCTE AFB170007 is greatly acknowledged. Saint-Gobain NorPro is acknowledged for kindly providing some of the catalyst supports.

References

1 M. Manzoli, F. Menegazzo, M. Signoretto and D. Marchese, *Catalysts*, 2016, **6**, 107.
2 K. Gupta, R. K. Rai and S. K. Singh, *ChemCatChem*, 2018, **10**, 2326–2349.
3 J. O. Odigure, A. S. Abdulkareem, A. Jimoh, J. O. Okafor and A. A. Abiodun, *Energy Sources Part Recovery Util. Environ. Eff.*, 2015, **37**, 1846–1852.
4 A. R. Zahedi, M. Rafizadeh and S. R. Ghafarian, *Polym. Int.*, 2009, **58**, 1084–1091.
5 S. Luo, X. Qiao, Q.-Y. Wang, Y.-F. Zhang, P. Fu, Z.-D. Lin, F.-P. Du and C. Cheng, *J. Mater. Sci.*, 2019, **54**, 5961–5970.
6 N. Gemmeke, M. Feldmann and H.-P. Heim, *Compos. Part Appl. Sci. Manuf.*, 2019, **118**, 327–335.
7 T. Qian, Y. Zhong, Z. Mao, H. Xu, L. Zhang, X. Sui and B. Wang, *J. Appl. Polym. Sci.*, 2019, **136**, 47330.
8 X. Hou, W. Zhang, M. He, Y. Lu, K. Lou and F. Gao, *Asian J. Pharm. Sci.*, 2017, **12**, 558–568.
9 R. Wojcieszak, F. Santarelli, S. Paul, F. Dumeignil, F. Cavani and R. V. Gonçalves, *Sustain. Chem. Process.*, 2015, **3**, 9.
10 W. Chu, J. Luo, S. Paul, Y. Liu, A. Khodakov and E. Bordes, *Catal. Today*, 2017, **298**, 145–157.
11 S. Benomar, A. Massó, B. Solsona, R. Issaadi and J. López Nieto, *Catalysts*, 2018, **8**, 126.
12 P. Hu, Y. Chen, X. Yan, W.-Z. Lang and Y.-J. Guo, *Ind. Eng. Chem. Res.*, 2019, **58**, 4065–4073.
13 A. M. Love, C. A. Carrero, A. Chieregato, J. T. Grant, S. Conrad, R. Verel and I. Hermans, *Chem. Mater.*, 2016, **28**, 5495–5504.
14 G. Lv, C. Chen, B. Lu, J. Li, Y. Yang, C. Chen, T. Deng, Y. Zhu and X. Hou, *RSC Adv.*, 2016, **6**, 101277–101282.
15 X. Li, P. Jia and T. Wang, *ACS Catal.*, 2016, **6**, 7621–7640.
16 J. Lan, Z. Chen, J. Lin and G. Yin, *Green Chem*, 2014, **16**, 4351–4358.
17 X. Li, B. Ho and Y. Zhang, *Green Chem.*, 2016, **18**, 2976–2980.
18 G. Lv, S. Chen, H. Zhu, M. Li and Y. Yang, *J. Clean. Prod.*, 2018, **196**, 32–41.
19 A. Chieregato, J. M. López Nieto and F. Cavani, *Coord. Chem. Rev.*, 2015, **301–302**, 3–23.
20 X. Li, J. Ko and Y. Zhang, *ChemSusChem*, 2018, **11**, 612–618.
21 N. Alonso-Fagúndez, M. L. Granados, R. Mariscal and M. Ojeda, *ChemSusChem*, 2012, **5**, 1984–1990.
22 N. Alonso-Fagúndez, M. Ojeda, R. Mariscal, J. L. G. Fierro and M. López Granados, *J. Catal.*, 2017, **348**, 265–275.
23 Andrei Khodakov, Bryan Olthof, Alexis T. Bell and Enrique Iglesia, *J. Catal.*, 1999, **181**, 205–216.
24 M. A. Betiha, A. M. Rabie, A. M. Elfadly and F. Z. Yehia, *Microporous Mesoporous Mater.*, 2016, **222**, 44–54.
25 A. Ruiz Puigdollers, P. Schlexer, S. Tosoni and G. Pacchioni, *ACS Catal.*, 2017, **7**, 6493–6513.
26 E. I. Kauppi, K. Honkala, A. O. I. Krause, J. M. Kanervo and L. Lefferts, *Top. Catal.*, 2016, **59**, 823–832.

27 P. Scherrer, in *Kolloidchemie Ein Lehrbuch*, Springer Berlin Heidelberg, Berlin, Heidelberg, 1912, pp. 387–409.
28 V. V. Kaichev, G. Ya. Popova, Yu. A. Chesalov, A. A. Saraev, T. V. Andrushkevich and V. I. Bukhtiyarov, *Kinet. Catal.*, 2016, **57**, 82–94.
29 R. Bulánek, A. Kalužová, M. Setnička, A. Zukal, P. Čičmanec and J. Mayerová, *Catal. Today*, 2012, **179**, 149–158.
30 J. M. Hidalgo, Z. Tišler, D. Kubička, K. Raabova and R. Bulanek, *J. Mol. Catal. Chem.*, 2016, **420**, 178–189.
31 J. Tauc, *Mater. Res. Bull.*, 1968, **3**, 37–46.
32 K. S. W. SING (UK, Chairman); D. H. EVERETT (UK);, R. A. W. HAUL (FRG); L. MOSCOU (Netherlands);, R. A. PIEROTTI (USA); J. ROUQUEROL (France); and T. SIEMIENIEWSKA, *Pure Appl Chem*, 1985, **57**, 603—619.
33 ELLIOT P. BARRETT, LESLIE G . JOYNER and PAUL P . HALENDA, *Vol. AREA Distrib. POROUS Subst.*, 1951, **73**, 373–380.
34 L. D. Gelb and K. E. Gubbins, *Langmuir*, 1999, **15**, 305–308.
35 M. Thommes, R. Köhn and M. Fröba, *J. Phys. Chem. B*, 2000, **104**, 7932–7943.
36 M. Yu, X. Lin, X. Li, M. Yan, B. Prabowo, W. Li, T. Chen and J. Yan, *Environ. Sci. Pollut. Res.*, 2016, **23**, 16249–16258.
37 E. V. Danilevich, G. Ya. Popova, T. V. Andrushkevich, V. V. Kaichev, I. G. Danilova, Yu. A. Chesalov, V. A. Rogov, V. I. Bukhtiyarov and V. N. Parmon, *Appl. Catal. Gen.*, 2014, **475**, 98–108.